Phonon diffraction and interference using nanometric features

Paul Desmarchelier, Efstrátios Nikidis, Roman Anufriev, Anne Tanguy, Yoshiaki Nakamura, Joseph Kioseoglou, Konstantinos Termentzidis

Phonon diffraction and interference using nanometric features

Paul Desmarchelier,[1,2] Efstrátios Nikidis,[3] Roman Anufriev,[1] Anne Tanguy,[4,5] Yoshiaki Nakamura,[6] Joseph Kioseoglou,[3] and Konstantinos Termentzidis[1]

[1)]*Univ Lyon, INSA Lyon, CNRS,CETHIL, UMR5008, 69621 Villeurbanne, France*

[2)]*Department of Materials Science & Engineering, Johns Hopkins University, Baltimore, Maryland 21218, USA*

[3)]*Physics Department, Aristotle University of Thessaloniki, GR-54124 Thessaloniki, Greece*

[4)]*ONERA, University Paris-Saclay, Chemin de la Hunière, BP 80100, 92123 Palaiseau, France*

[5)]*Univ Lyon, INSA Lyon, CNRS, LaMCoS, UMR5259,69621 Villeurbanne, France*

[6)]*OSAKA University, 560-8531 Osaka, Japan*

(*pdesmar2@jh.edu)

(Dated: 22 November 2023)

Phonon diffraction and interference patterns are observed at the atomic scale, using molecular dynamics simulations in systems containing crystalline silicon and nanometric obstacles such as voids or amorphous inclusions. The diffraction patterns due to these nano-architectured systems of the same scale as the phonon wavelengths are similar to the ones predicted by the simple Fresnel-Kirchhoff integral. The few differences between the two approaches are attributed to the nature of the interface and the anisotropy of crystalline silicon. Based on the wave description of phonons, these findings can provide insights on the interaction of phonons with nano-objects and can have applications in smart thermal energy management.

I. INTRODUCTION

Diffraction and interference can be observed for any kind of wave propagation and have been studied since the sixteenth century for light[1], the most famous example being Young's double slit experiment[2]. Diffraction is well described since the end of the nineteenth century through the Fresnel-Kirschoff equation[3]. It relates the wavelength and the geometry of the aperture through which the wave is diffracted to compute the resulting wave amplitude as a function of position. This relation is commonly used in optics, as well as in acoustics and geophysics[4]. Indeed, this model is valid for any kind of propagating wave, including electromagnetic waves (photons) and lattice vibrations (phonons) in homogeneous and isotropic media.

The first experiments showing phonon interferences, or more broadly interference of high-frequency propagative waves in solids, date from the second half of the last century: with for instance the work of Anderson and Sabisky[5]. Since then, phonon interferences have been used to engineer phonon bandgaps in superlattices or phononic crystals[6–9]. Recently, interference was induced by creating two phonon pathways that interact with each other, decreasing the transmission of specific frequencies[10]. More recently, interference of low THz wave-packets has been shown in computer simulated phononic crystals[11]. More globally, the importance of the wavelike nature of phonons, is highlighted in recent reviews[12,13]. Phonon interference is relevant for energy applications because the patterns have an influence on the spatial distribution of energy, creating cold and hot spots.

Defects can affect the direction of propagation of phonons via diffraction, which can also influence lattice heat conduction at frequencies contributing significantly to the heat transfer ($\sim$THz). For example, it has been shown that dislocation arrays can act as a diffraction grating[14]. Diffraction has also been evidenced by the interference patterns induced by periodic transducers in pump-probe experiments, as shown by their influence on conductance[15] or visualization of the pattern via angle-resolved Brillouin scattering[16]. Finally, the effect of phonons diffraction on thermal transfer has been shown experimentally[17] and described theoretically for a single constriction[18].

However, the existing studies either focus on the indirect consequences of diffraction and interference or on low-frequency phonons. Even though terahertz range coherent phonons can be obtained[19], it is challenging to observe the spatially resolved diffraction and interference of phonons directly, the usual methods relying on indirect effects, such as the impact on the conductance[15]. This limitation can be overcome by using Molecular Dynamics (MD) simulations that

give access to the different quantities at the atomic scale, such as the kinetic energy of each atom, enabling the direct visualization of high-frequency waves.

Experimentally, diffraction is obtained thanks to the shape of the transducer[15–17], or natural or engineered dislocations[14]. With the progress of nano-structuration, it is also possible to fabricate crystalline nanometric windows through nanometric thick amorphous layers[20–22]. These later nanocomposites were the motivation to study the diffraction/interference phenomena of a wavepacket by nanometric crystalline apertures. The properties of crystalline/amorphous nanocomposites are affected by the structuration[23], and the interaction between the phases[24]. In particular, it has been shown that structures containing amorphous parts affect sufficiently the propagation of phonons to create weak-to-strong scattering transitions in this frequency range, and thus phonon propagation in the amorphous barrier is hindered[25].

In this article, we will uncover that both diffraction and interference phenomena of TeraHertz range phonons can be induced by nanometric apertures in voids or amorphous silicon barriers in a bulk crystalline silicon. After a brief description of the MD simulations, we focus on the diffraction phenomena, then on the emerging interference pattern, and finally discuss the limitations and implications of the findings.

II. METHOD

To study the propagation and diffraction of a 6 THz longitudinal wave, we use a crystalline silicon slab in which a nanometric barrier with a small aperture is introduced. This barrier consists of a void (air gap) or amorphous silicon (a-Si). The pristine silicon slab has the $\langle 100 \rangle$ direction aligned with the z axis, the barrier has a thickness A of 1 nm if it is a void and of 8 nm if it is amorphous. A schematic view of the geometry is proposed in figure 1. In other words, a diffraction grating is built using nanometric crystalline bridges over a void or a thin a-Si layer. As diffraction occurs when the size of the obstacle is of the order of the wavelength, we set the width of the channel to c= 3 nm. For reference, the wavelength in c-Si at 6 THz is 1.2 nm (for longitudinal phonon in the $\langle 100 \rangle$ direction). This value is extracted from the dispersion relation for the specific interatomic potential used[26], using the dynamical structure factor (the exact method is described in a previous article[27]).

To reproduce an infinite medium, periodic boundary conditions are used in the width (x) and depth (y) directions, while fixed boundary conditions are used in the propagation direction (z) to

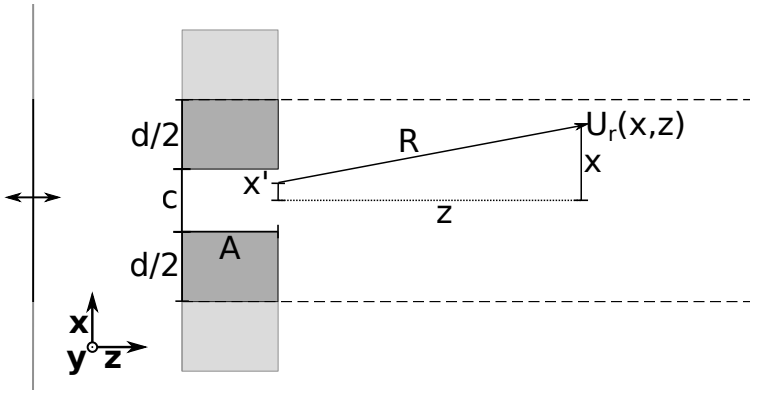

FIG. 1. Schematic representation of the system with the parameters used for equation [1], the gray area represents the barrier (void or a-Si), the dashed lines show the periodic boundary condition, and the vertical line with an arrow is the zone where phonons are excited.

prevent interference in this direction and mitigate the free surface effect. As a result, we obtain a transmission diffraction grating with an infinite number of apertures equally spaced along x. The apertures (here channels through the barrier) are infinitely long in y. The diffracted wave exiting the channel interacts with its image waves through the periodic boundary conditions in x. To depict this phenomenon, we have chosen a rather large length after the channel exit (here 120 nm). The dimensions of the simulation box are 200 nm in length, 47 nm in width, and 4 nm in thickness. The MD software LAMMPS is used to run the simulations[28].

It is worth noting that nanometric crystalline windows in an amorphous barrier, similar to what is described here, can be obtained experimentally: the group of Y. Nakamura masters the growth of periodic nanostructures containing amorphous and crystalline phases with nanometric bridges over the amorphous layers[21,22,29,30].

The wave is created by exciting a 4 Å thick slice with a sinusoidal force excitation in the z direction, this slice position is represented in figure 1 by the vertical black line on the left with the arrows showing the polarization of the excitation (longitudinal). As mentioned previously, the frequency is set at 6 THz as its wavelength (1.2 nm) corresponds to the order of the aperture size. The amplitude of the excitation is very low and results in a maximal local displacement of 1×10^{-4} Å, such a low excitation amplitude is possible because the system is at mechanical equilibrium at the beginning of the simulation (T= 0 K). This study focuses only on the propagation of the wave after the aperture in the $z+$ direction before it reaches the boundary of the simulation box in z.

The MD model used is accompanied by a simple 2D diffraction model based on the Fresnel-

Kirchhoff equation[31] assuming a superposition of emitted spherical (here circular) waves at the aperture opening:

$$U_r(x,z) = K\int_{-c/2}^{c/2} U_r(x',0)\frac{exp(ikR)}{R}\left[\frac{1+R/z}{2}\right]dx' \tag{1}$$

with dx' the integral over the aperture, $R=\sqrt{(x-x')^2+z^2}$, $k=2\pi/\lambda$ (λ being the wavelength), and K the amplitude. Note that, thanks to translation invariance in the MD model, there is no need to treat the third dimension. The different geometrical parameters are defined in figure 1. The origin of the z axis is set at the aperture opening, and the origin of the x-axis is taken at the center of the aperture. To compute the full displacement field, the integral is computed for each point in a grid of dimensions corresponding to the MD simulations, with a resolution of dz=1.6 Å and dx=1.1 Å. The integral is solved using a Clenshaw–Curtis method implemented in SciPy[32]. $U_r(x',0)$ is here defined as a constant, which is equivalent to assuming a (space) uniform displacement at the exit of the channel. The interface effects in the channel are neglected. Another assumption made using equation [1] is that wave-propagation is isotropic, with the anisotropy of c-Si being neglected. Note that, due to the intermediate size of the system, the small angle approximation does not hold, and neither the Frauenhofer nor the Fresnel approximations can be used to compute the pattern from the aperture to the end of the slab[31].

Because the displacement is a sinusoid, the kinetic energy associated with the wave can be obtained to a multiplication factor simply by using the square of the displacement:

$$E_k(x,z) \propto U_r^2(x,z) \tag{2}$$

Equation 1 gives the diffraction by a single aperture, to obtain the solution for multiple apertures, one can sum the displacement field obtained for each aperture. The results shown use the superposition of five apertures shifted according to the periodic boundary conditions.

III. RESULTS

In this section, we will present the results of both models, MD and Fresnel-Kirchhoff equation-based, starting with diffraction and then focusing on the interferences.

A. Diffraction

The phonon diffraction can be directly represented by the visualization of the atomic kinetic energy, as shown in figure 2 with the propagation of a continuous wave, diffracted by an aperture in a void barrier. The kinetic energy is used to visualize the shape of the waves rather than the displacements, which eases the post-processing. The diffraction phenomenon appears clearly with a central ray that slowly broadens as it propagates in zone 1 of figure 2. The secondary diffraction lobes are also visible in zones labeled 2, which is a first sign that the phenomenon is very close to textbook diffraction[31].

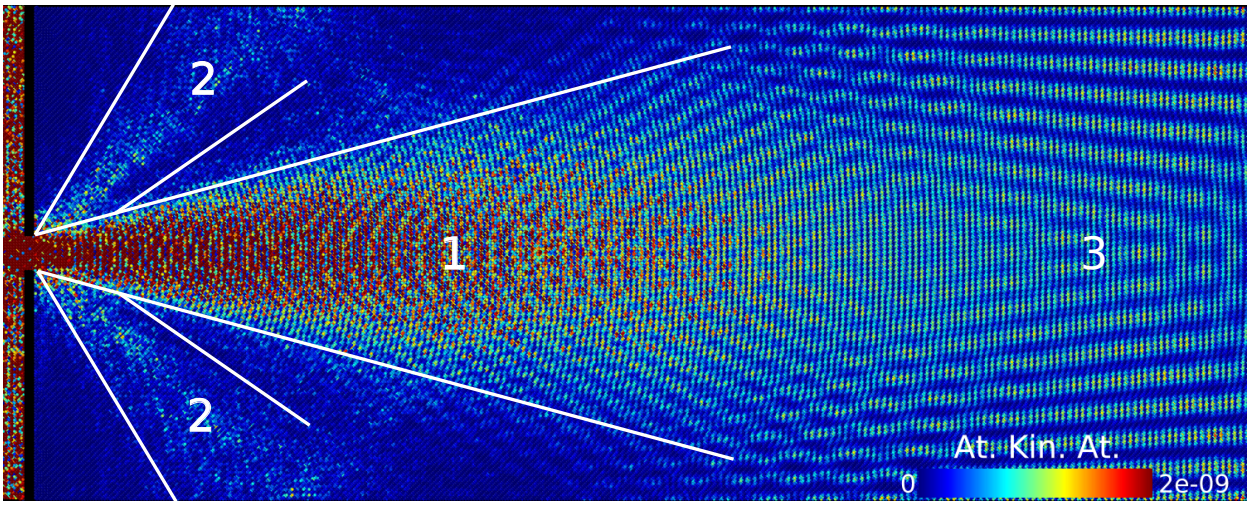

FIG. 2. Visualization of diffraction of a 6 THz continuous longitudinal plane wave by an aperture of a width of 3 nm using a void barrier. The color scale represents the kinetic energy per atom in eV. 1, 2 and 3 denote areas of interest explained in the main text.

For further analysis, the diffraction patterns computed via equation [1], and obtained with the MD models with a void barrier as well as the a-Si barrier are represented in figure 3. To enhance the pattern, the color scale is normed, for each pixel column along z, by the highest value in the pixel column for each panel. With this representation, the central (1) and lateral (2) diffraction lobes observed in figure 2 appear clearly for both the MD with a void barrier and the model based on equation [1]. Confirming that we have a usual diffraction pattern. However, for the a-Si barrier, there is more noise due to the diffusion of energy through the amorphous barrier, and the lateral lobes are not visible (a complementary visualization of this configuration is given in appendix A). Nonetheless, the slowly broadening central ray characteristic of diffusion can be distinguished. It

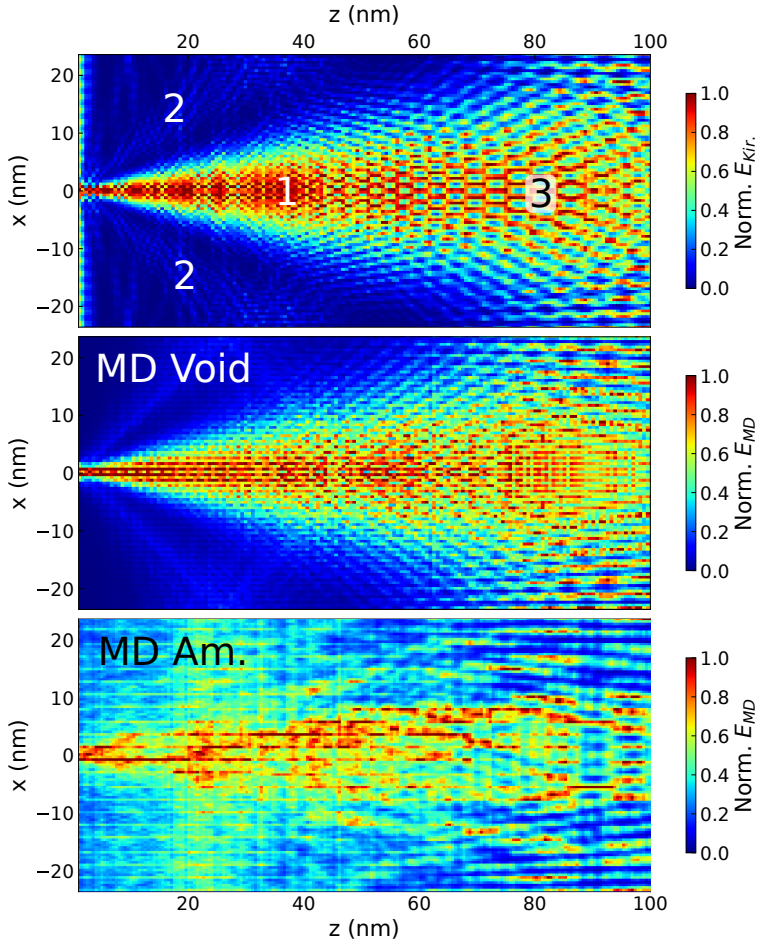

FIG. 3. Comparison of the results obtained with the Kirchhoff integral (top) and the MD simulation with a void barrier (middle) and an amorphous barrier (bottom), with color representing the kinetic energy. 1, 2 and 3 denote areas of interest explained in the main text. The energy value is normalized by the maximum value for each pixel column along z.

also appears that the a-Si barrier results in a broader ray at the exit of the channel than the void barrier. This probably comes from the a-Si/c-Si interface allowing the transmission of energy[33]. Note that the band appearing at z=20 nm is most likely an artifact due to the normalization. Indeed, at this distance, the energy diffused through the barrier and the one diffracted by the aperture are similar. Closer to the barrier, the diffracted wave dominates, and the diffusion did not reach further away past 30 nm, as a result, the diffracted ray dominates. This is corroborated by the absence of such a band in appendix A.

A comparison of the predicted patterns for the Fresnel-Kirchhoff law and the MD simulation at different distances is proposed in figure 4 and 5. In figure 4 at 10 nm, it appears that once scaled,

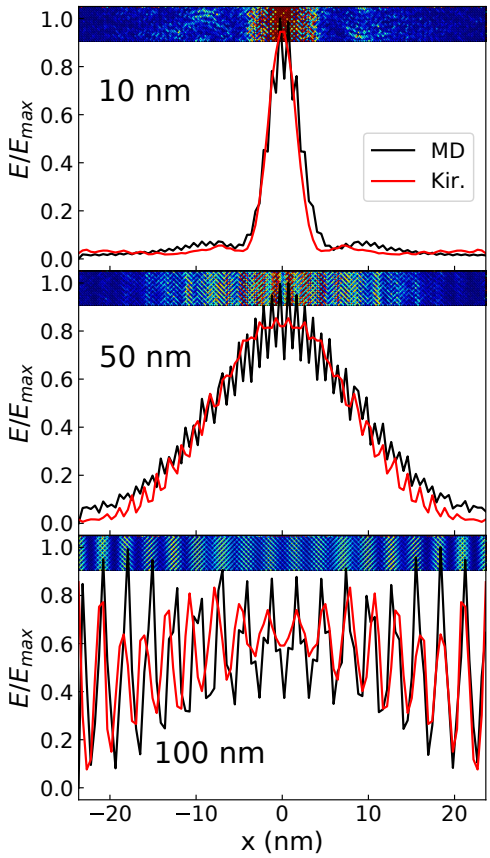

FIG. 4. Kinetic energy distribution along the x-axis at z=10, 50 and 100 nm of the MD simulation with a void barrier (full black line) and the Kirchhoff model in red. The insets give an atomic representation of the same quantity with the same color scale as figure 2 (blue is zero and red is 2e-09 eV/atom)

the two curves match, principally for the central lobe but also for the lateral lobes, with minimal discrepancy. At 50 nm, again, the central lobe matches. In the case of the amorphous barrier, in figure 5, due to the higher thermal noise caused by the energy diffusing through the barrier, the pattern matches less well, with only the central peak visible.

Thanks to a comparison of a MD and a Fresnel-Kirchhoff equation-based model, we have shown that a high-frequency impulsion can be diffracted by a nanometric aperture in a void or amorphous barrier. In the next section, we show that this diffracted wave interferes with itself through the periodic boundary conditions.

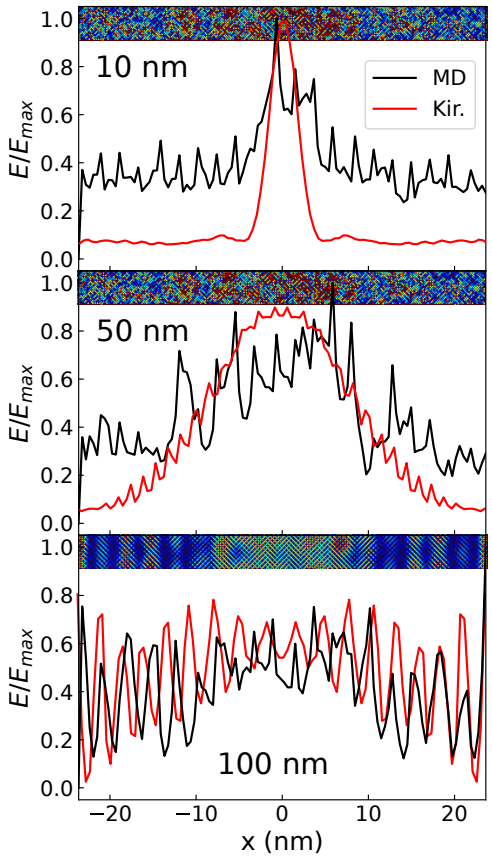

FIG. 5. Kinetic energy distribution along the x-axis at z=10, 50 and 100 nm of the MD simulation with an a-Si barrier (full black line) and the Kirchhoff model in red. The insets give an atomic representation of the same quantity with the same color scale as figure 2 (blue is zero and red is 2e-09 eV/atom)

B. Interference

Through figures 2 and 6 the interference pattern appears as slanted lines (zone 3) as expected for a far field interference pattern. It can also be noted that the patterns observed with equation [1] and with the MD simulation with a void barrier are very similar: first visually in figure 3 and also in the bottom panel of figure 4. The prediction of the pattern using equation [1] matches notably in terms of the position and numbers of the peaks, with only a slight shift. This shift may be attributed to the discretization due to the atomic nature of the matter or to the computation grid. It also appears that as one gets further away from the aperture, the amplitude of the different peaks starts to differ between the two models, this may be understood as an effect of group velocity anisotropy in c-Si favoring some directions. The wave exiting the channel may also not be uniform at the opening, as supposed in the Fresnel-Kirchhoff model. Indeed, the free surface may impact the propagation,

as suggested for nanowires[27]. Importantly, in the amorphous barrier case in the lower panel of figure 5, the positions of the high-intensity fringes still match the Fresnel-Kirchhoff predicted one, in particular further away from the center. This indicates that the previous discrepancies 10 and 50 nm away from the aperture are indeed caused by the thermal noise caused by the permeability of the amorphous barrier.

IV. DISCUSSION AND CONCLUSION

We have shown that an array of channels across voids or amorphous patches creates a diffraction pattern very similar to the one predicted by the Kirchhoff integral for a TeraHertz range compression wave. The global shape of the patterns, as well as the number and position of interference fringes, are reproduced.

It is noteworthy that equation 1 is able to predict the relative energy distribution from the near to the far field, as shown in figure 4. This shows that most of the phenomenon is captured by the simple model using equation [1]. More striking is that this still holds for a partially permeable amorphous membrane of a-Si, the same features are visible in figure 5 with more thermal noise.

Despite the above similarities, there are a few differences between the patterns obtained through the equation [1] and the ones obtained with the MD simulation. When looking at the details at z= 100 nm in figure 4 it appears that even though the number of fringes between the two models matches, their positions are slightly phase shifted, and their amplitudes do not match. This may be, again, due to the anisotropy. Indeed, crystalline Si is anisotropic[34]. This anisotropy is not included in equation [1] that assumes that the medium is isotropic. The treatment of anisotropy for diffraction in the near field exceeds the scope of this work. It also appears clearly that the spatial pattern of the kinetic energy resulting from MD simulations is less sharp and contrasted than the one using the equation [1]. This can be explained by the continuous medium model that has been used for the implementation of the wave propagation, which contrasts with the discrete atomistic nature of the materials and the MD simulations.

The choice of the different parameters is made to observe interference due to sub-10-nm features, and their influence is worth discussing. The ratio of c to the wavelength will determine how pronounced the diffraction is, that is, how close the diffracted wave is to resembling a single cylindrical wave at the aperture. A very large aperture opening c will barely diffract the incoming wave, and it will keep its plane wave characteristics, only the edges will be affected. As such, any phonon

can form a diffraction pattern as long as c is of the same order of magnitude as the wavelength, as shown for micrometric apertures and GHz waves in the work of Dieleman et al.[16]. Varying d will not affect the diffraction, but the interference pattern will change because the distance between the holes is affected. Finally, a variation of A should theoretically not affect the interference pattern. However, other phenomena may appear due to interaction with the free surface or interface. A study of the effect of the interface parallel to the propagation on the propagation of waves (in nanowires) may be found in an earlier work[27]. Also, any phonon polarization could potentially create interference patterns, as shown in appendix C for a transverse excitation.

It is important to keep in mind that the simulations in this article are performed at very low temperatures, with the sinusoidal excitation as the only source of energy to minimize the thermal noise. This facilitates the visualization of the results: at higher temperatures, the kinetic energy used to visualize the interference patterns would be dominated by noise. Nevertheless, since the length scale involved is lower than the mean free path in c-Si, we expect that the same phenomena will appear at a finite temperature. The only prerequisite to observe the phenomena directly is that the high-energy fringes have higher energy than the thermal noise, this can be done by averaging over multiple simulations or a long time and increasing the excitation amplitude. An example at 25 K with a higher amplitude is provided in figure 9. However, perhaps more importantly, an effect of a nanometric diffraction grating on the conductance has already been observed experimentally at 1 K [15] or at room temperature using GHz range phonons[16].

As stated above, structures similar to the ones described in this article have already been obtained experimentally[21,22,29,30]. Such structures could have practical applications: using the diffraction of lower wavelength, a phonon high-pass filter can be obtained. Moreover, the diffraction by small obstacles could be used to design phonon lenses, as described for acoustic waves by Gupta and Ye[35].

One of the takeaways of this study is that the interference phenomenon could matter. Specifically, taking into account phonon interference can improve studies that use phonon Monte Carlo simulations. Indeed, by design, Monte Carlo simulations treat phonons as quasi-particles and cannot observe phonon interference patterns, as shown in appendix B.

To conclude, we have shown using MD that voids or amorphous patches can cause diffraction and interference patterns for waves at frequencies that are important for thermal transport in c-Si. These interference patterns can be reasonably predicted using the Fresnel-Kirchhoff equation, with some discrepancies due to anisotropy. Due to its simplicity, the model is robust and might

be applied at larger or smaller scales and at different frequencies. However, it ignores the specificities of the barrier surfaces and the anisotropy effects that are detailed in this article. This study indicates that the wave nature of phonons matters even at high frequencies in crystals. This might also be important for phonon focusing applications, where phononic crystals are studied using an approach that considers phonons as particles[36].

ACKNOWLEDGMENTS

This work was granted access to the HPC resources of IDRIS under the allocation 2021-A0110911092, made by GENCI, and also granted access from the Greek Research and Technology Network (GRNET) in the National HPC facility -ARIS- under the project NOUS(pr012041).This work was supported in part by NSF Grant No. PHY-1748958 and the Gordon and Betty Moore Foundation Grant No. 2929.02. The authors want to thank fruitful discussions with Carsten HENKEL, Gabriel DUTIER and Yanguy GUO.

DATA AVAILABILITY STATEMENT

The data that support the findings of this study are available from the corresponding author upon reasonable request.

Appendix A: Atomic Visualization for Amorphous Barrier

Figure 6 is very similar to figure 2 to the difference that an amorphous barrier is used. This barrier is partially permeable to the energy emanating from the excitation zone. As a result, some of the energy diffuses through the barrier, explaining why the color scale is saturated in the first half.

Appendix B: Monte-Carlo simulation

To emphasize the role of the wave nature of phonons, the MD simulations can be compared to the results obtained using quasi-particle approach, Monte-Carlo for phonons using FreePATHS package. An example is given in figure 7, phonons, as considered particles, are drawn from the equilibrium distribution at 4 K from a thermal bath situation before the aperture (the white zone

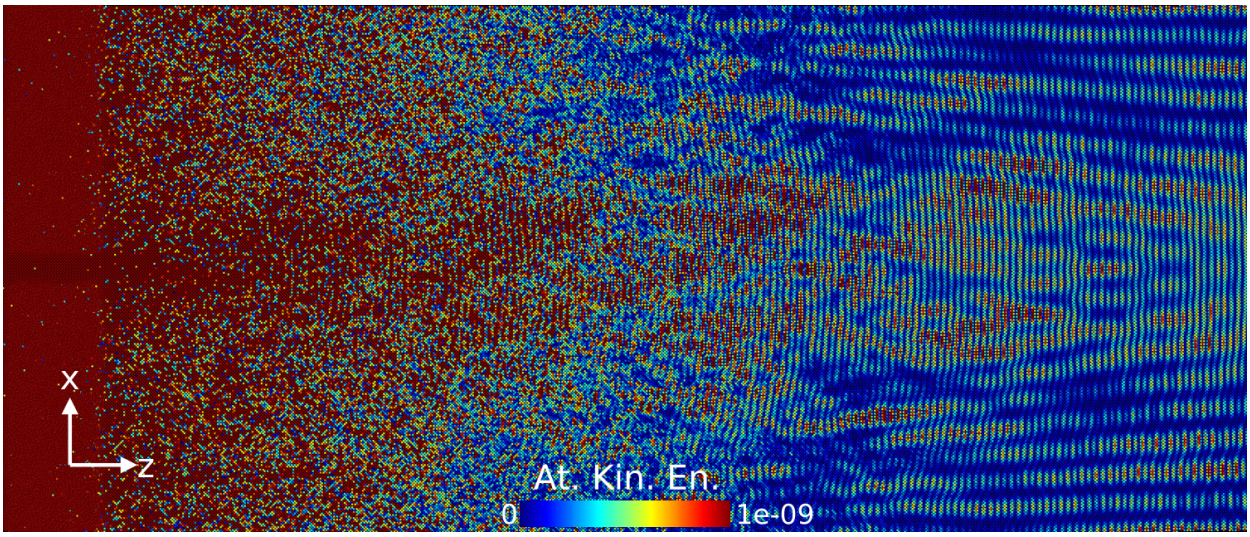

FIG. 6. Visualization of diffraction of a 6 THz continuous longitudinal plane wave by an aperture of a width of 3 nm using an amorphous barrier. The color scale represents the kinetic energy per atom in eV.

before the channel). Their direction is also chosen randomly from the dispersion curves of silicon, the method used here is detailed in the study of Anufriev et al.[36].

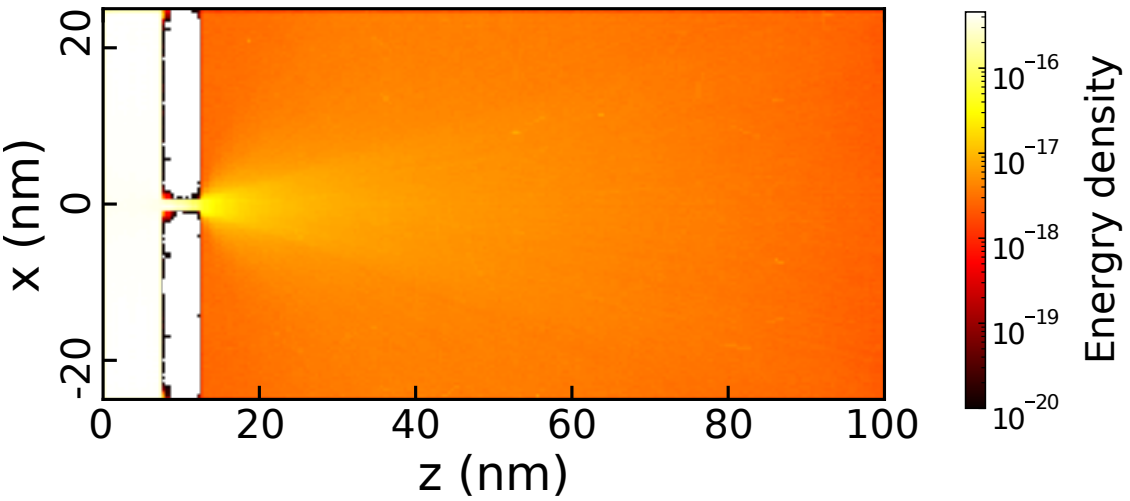

FIG. 7. Same configuration as presented in figure 2 simulated with the Monte-Carlo method.

A widening of the ray exiting the channel is visible; however, it comes from the phonon not propagating perfectly parallel to the z axis either due to reflection in the channel or their original direction, not from diffraction as it is not included in the model. This is confirmed by the absence of the lateral lobes. Moreover, no signs of interference are visible, there are no parallel lines emerging in the far field, and the energy distribution starts to be homogeneous.

Appendix C: Transverse excitation

Figure 8 provides a visualization of the kinetic energy distribution in the crystal after a 3 THz transverse acoustic excitation (polarized along y). It shows that the diffraction/interference pattern can be observed for longitudinal as well as transverse phonons. The choice of 3 THz is arbitrary to obtain a wavelength roughly similar to the one at 6 THz for longitudinal polarization. However, the wavelength is not exactly the same (1.6 vs. 1.2 nm) explaining the difference in the pattern.

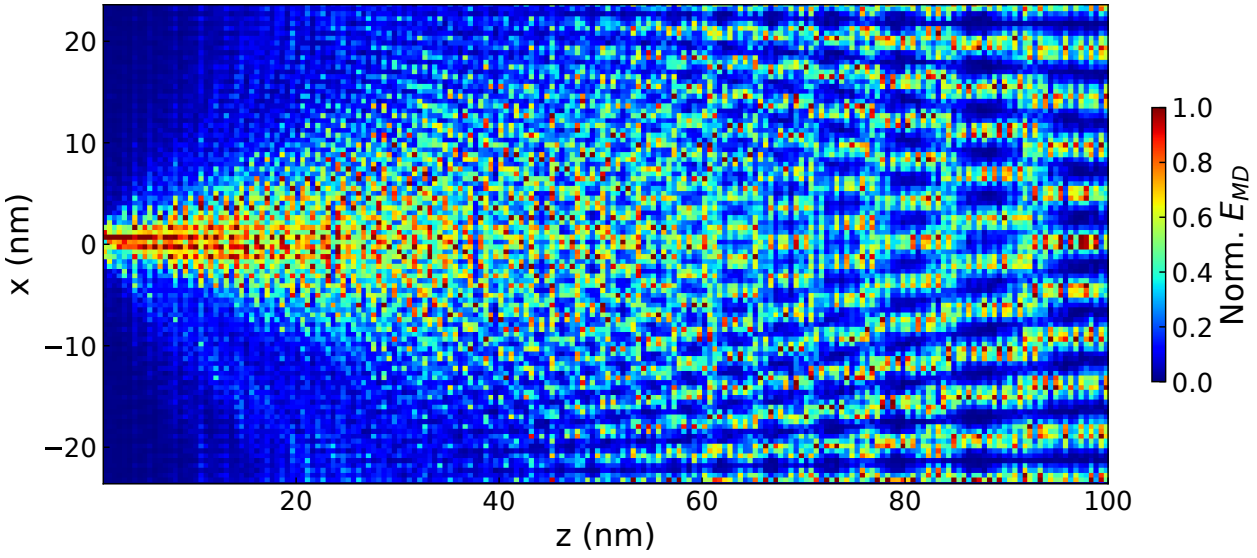

FIG. 8. Visualization of the diffraction/interference pattern caused by a 3 THz continuous transverse plane wave going through an aperture of a width of 3 nm using a void barrier. The energy value is normalized by the maximum value for each pixel column along z.

Appendix D: Finite Temperature

In the main text, the simulations are performed at 0K to ease visualization, but the same simulation can be performed at a finite temperature. An example at 25 K is given in figure 9, with the same configuration and normalization as for figure 3. The same features appear with more background noise due to the higher temperature. This temperature was chosen because it is possible to obtain the interference/diffraction figure with an increased excitation amplitude (circa 2000 times the original one). The continuous excitation increases the temperature significantly, up to 1000 K. This effect could be mitigated by limiting the excitation duration and averaging over multiple simulations with a lower excitation amplitude.

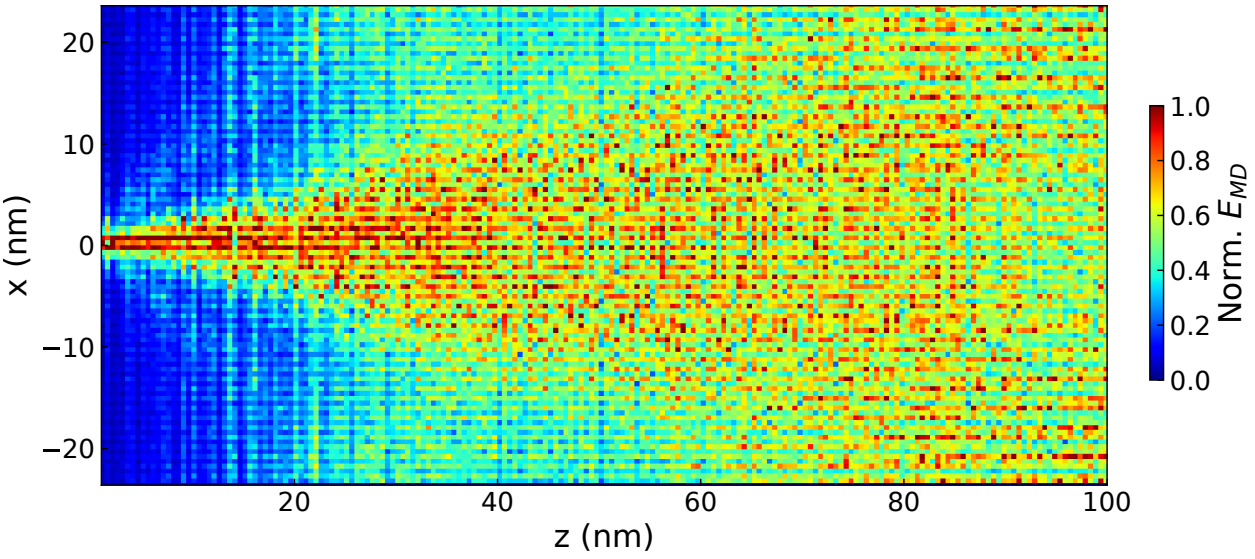

FIG. 9. Visualization of the diffraction and interference patterns created by a 6 THz continuous longitudinal plane wave going through an aperture of a width of 3 nm using a void barrier at 25 K. The energy value is normalized by the maximum value for each pixel column along z.

REFERENCES

[1]C. Huygens, *Traité de la lumière* (Gauthier-Villars, 1920).

[2]T. Young, "Ii. the bakerian lecture. on the theory of light and colours," Philosophical Transactions of the Royal Society of London **92**, 12–48 (1802), https://royalsocietypublishing.org/doi/pdf/10.1098/rstl.1802.0004.

[3]G. Kirchhoff, "Zur theorie der lichtstrahlen," Annalen der Physik **254**, 663–695 (1883), https://onlinelibrary.wiley.com/doi/pdf/10.1002/andp.18832540409.

[4]S. M. Deregowski and S. M. Brown, "A theory of acoustic diffractors applied to 2-d models*," Geophysical Prospecting **31**, 293–333 (1983).

[5]C. H. Anderson and E. S. Sabisky, "Phonon interference in thin films of liquid helium," Phys. Rev. Lett. **24**, 1049–1052 (1970).

[6]G. Xie, Y. Guo, X. Wei, K. Zhang, L. Sun, J. Zhong, G. Zhang, and Y.-W. Zhang, "Phonon mean free path spectrum and thermal conductivity for $si_{1-x}ge_x$ nanowires," Applied Physics Letters **104**, 233901 (2014), https://doi.org/10.1063/1.4882083.

[7]X. Wang, M. Wang, Y. Hong, Z. Wang, and J. Zhang, "Coherent and incoherent phonon transport in a graphene and nitrogenated holey graphene superlattice," Phys. Chem. Chem. Phys. **19**,

24240–24248 (2017).

[8]E. Chavez-Angel, P. Tsipas, P. Xiao, M. T. Ahmadi, A. H. S. Daaoub, H. Sadeghi, C. M. Sotomayor Torres, A. Dimoulas, and A. E. Sachat, "Engineering heat transport across epitaxial lattice-mismatched van der waals heterointerfaces," Nano Letters **23**, 6883–6891 (2023), pMID: 37467035, https://doi.org/10.1021/acs.nanolett.3c01280.

[9]S. Valiya Valappil, A. M. Aragón, and H. Goosen, "Phononic crystals' band gap manipulation via displacement modes," Solid State Communications **361**, 115061 (2023).

[10]S. Hu, L. Feng, C. Shao, I. A. Strelnikov, Y. A. Kosevich, and J. Shiomi, "Two-path phonon interference resonance induces a stop band in a silicon crystal matrix with a multilayer array of embedded nanoparticles," Phys. Rev. B **102**, 024301 (2020).

[11]Y. Li, A. Diaz, X. Chen, D. L. McDowell, and Y. Chen, "Interference, scattering, and transmission of acoustic phonons in si phononic crystals," Acta Materialia **224**, 117481 (2022).

[12]M. Simoncelli, N. Marzari, and F. Mauri, "Unified theory of thermal transport in crystals and glasses," Nature Physics **15**, 809–813 (2019).

[13]Z. Zhang, Y. Guo, M. Bescond, J. Chen, M. Nomura, and S. Volz, "Heat conduction theory including phonon coherence," Phys. Rev. Lett. **128**, 015901 (2022).

[14]R. Hanus, A. Garg, and G. J. Snyder, "Phonon diffraction and dimensionality crossover in phonon-interface scattering," Communications Physics **1**, 1–11 (2018).

[15]P. D. Vu, J. R. Olson, and R. O. Pohl, "Phonon diffraction gratings," Annalen der Physik **507**, 9–25 (1995), https://onlinelibrary.wiley.com/doi/pdf/10.1002/andp.19955070103.

[16]D. J. Dieleman, A. F. Koenderink, A. F. M. Arts, and H. W. de Wijn, "Diffraction of coherent phonons emitted by a grating," Phys. Rev. B **60**, 14719–14723 (1999).

[17]M. P. Zaitlin and A. C. Anderson, "Phonon thermal transport in noncrystalline materials," Phys. Rev. B **12**, 4475–4486 (1975).

[18]R. Prasher, T. Tong, and A. Majumdar, "Diffraction-limited phonon thermal conductance of nanoconstrictions," Applied Physics Letters **91**, 143119 (2007), https://doi.org/10.1063/1.2794428.

[19]M.-C. Lee, N. Sirica, S. W. Teitelbaum, A. Maznev, T. Pezeril, R. Tutchton, V. Krapivin, G. A. de la Pena, Y. Huang, L. X. Zhao, G. F. Chen, B. Xu, R. Yang, J. Shi, J.-X. Zhu, D. A. Yarotski, X. G. Qiu, K. A. Nelson, M. Trigo, D. A. Reis, and R. P. Prasankumar, "Direct observation of coherent longitudinal and shear acoustic phonons in taas using ultrafast x-ray diffraction," Phys. Rev. Lett. **128**, 155301 (2022).

[20]Y. Nakamura, M. Isogawa, T. Ueda, S. Yamasaka, H. Matsui, J. Kikkawa, S. Ikeuchi, T. Oyake, T. Hori, J. Shiomi, and A. Sakai, "Anomalous reduction of thermal conductivity in coherent nanocrystal architecture for silicon thermoelectric material," Nano Energy **12**, 845–851 (2015).

[21]Y. Nakamura, "Nanostructure design for drastic reduction of thermal conductivity while preserving high electrical conductivity," Science and Technology of Advanced Materials **19**, 31–43 (2018), pMID: 29371907, https://doi.org/10.1080/14686996.2017.1413918.

[22]S. Yamasaka, Y. Nakamura, T. Ueda, S. Takeuchi, and A. Sakai, "Phonon transport control by nanoarchitecture including epitaxial ge nanodots for si-based thermoelectric materials," Scientific reports **5**, 1–9 (2015).

[23]K. Termentzidis, V. M. Giordano, M. Katsikini, E. Paloura, G. Pernot, M. Verdier, D. Lacroix, I. Karakostas, and J. Kioseoglou, "Enhanced thermal conductivity in percolating nanocomposites: a molecular dynamics investigation," Nanoscale **10**, 21732–21741 (2018).

[24]A. Tlili, V. M. Giordano, Y. M. Beltukov, P. Desmarchelier, S. Merabia, and A. Tanguy, "Enhancement and anticipation of the ioffe–regel crossover in amorphous/nanocrystalline composites," Nanoscale **11**, 21502–21512 (2019).

[25]Y. M. Beltukov, D. A. Parshin, V. M. Giordano, and A. Tanguy, "Propagative and diffusive regimes of acoustic damping in bulk amorphous material," Phys. Rev. E **98**, 023005 (2018).

[26]R. Vink, G. Barkema, W. van der Weg, and N. Mousseau, "Fitting the stillinger–weber potential to amorphous silicon," Journal of Non-Crystalline Solids **282**, 248–255 (2001).

[27]P. Desmarchelier, A. Tanguy, and K. Termentzidis, "Thermal rectification in asymmetric two-phase nanowires," Phys. Rev. B **103**, 014202 (2021).

[28]S. Plimpton, "Fast parallel algorithms for short-range molecular dynamics," Journal of Computational Physics **117**, 1–19 (1995).

[29]Y. Nakamura, M. Isogawa, T. Ueda, S. Yamasaka, H. Matsui, J. Kikkawa, S. Ikeuchi, T. Oyake, T. Hori, J. Shiomi, and A. Sakai, "Anomalous reduction of thermal conductivity in coherent nanocrystal architecture for silicon thermoelectric material," Nano Energy **12**, 845–851 (2015).

[30]S. Yamasaka, K. Watanabe, S. Sakane, S. Takeuchi, A. Sakai, K. Sawano, and Y. Nakamura, "Independent control of electrical and heat conduction by nanostructure designing for si-based thermoelectric materials," Scientific Reports **6**, 1–8 (2016).

[31]J. Peatross and M. Ware, *Physics of Light and Optics* (2015) p. JWA64.

[32]P. Virtanen, R. Gommers, T. E. Oliphant, M. Haberland, T. Reddy, D. Cournapeau, E. Burovski, P. Peterson, W. Weckesser, J. Bright, S. J. van der Walt, M. Brett, J. Wilson, K. J. Millman,

N. Mayorov, A. R. J. Nelson, E. Jones, R. Kern, E. Larson, C. J. Carey, İ. Polat, Y. Feng, E. W. Moore, J. VanderPlas, D. Laxalde, J. Perktold, R. Cimrman, I. Henriksen, E. A. Quintero, C. R. Harris, A. M. Archibald, A. H. Ribeiro, F. Pedregosa, P. van Mulbregt, and SciPy 1.0 Contributors, "SciPy 1.0: Fundamental Algorithms for Scientific Computing in Python," Nature Methods **17**, 261–272 (2020).

[33]L. Yang, B. Latour, and A. J. Minnich, "Phonon transmission at crystalline-amorphous interfaces studied using mode-resolved atomistic green's functions," Phys. Rev. B **97**, 205306 (2018).

[34]M. A. Hopcroft, W. D. Nix, and T. W. Kenny, "What is the young's modulus of silicon?" Journal of Microelectromechanical Systems **19**, 229–238 (2010).

[35]B. C. Gupta and Z. Ye, "Theoretical analysis of the focusing of acoustic waves by two-dimensional sonic crystals," Phys. Rev. E **67**, 036603 (2003).

[36]R. Anufriev and M. Nomura, "Ray phononics: Thermal guides, emitters, filters, and shields powered by ballistic phonon transport," Materials Today Physics **15**, 100272 (2020).